AEM
Journals.ASM.org

Semiquantitative Performance and Mechanism Evaluation of Carbon Nanomaterials as Cathode Coatings for Microbial Fouling Reduction

Qiaoying Zhang, Joanne Nghiem, Gregory J. Silverberg, Chad D. Vecitis

School of Engineering and Applied Sciences, Harvard University, Cambridge, Massachusetts, USA

In this study, we examine bacterial attachment and survival on a titanium (Ti) cathode coated with various carbon nanomaterials (CNM): pristine carbon nanotubes (CNT), oxidized carbon nanotubes (O-CNT), oxidized-annealed carbon nanotubes (OA-CNT), carbon black (CB), and reduced graphene oxide (rGO). The carbon nanomaterials were dispersed in an isopropyl alcohol-Nafion solution and were then used to dip-coat a Ti substrate. *Pseudomonas fluorescens* was selected as the representative bacterium for environmental biofouling. Experiments in the absence of an electric potential indicate that increased nanoscale surface roughness and decreased hydrophobicity of the CNM coating decreased bacterial adhesion. The loss of bacterial viability on the noncharged CNM coatings ranged from 22% for CB to 67% for OA-CNT and was dependent on the CNM dimensions and surface chemistry. For electrochemical experiments, the total density and percentage of inactivation of the adherent bacteria were analyzed semiquantitatively as functions of electrode potential, current density, and hydrogen peroxide generation. Electrode potential and hydrogen peroxide generation were the dominant factors with regard to short-term (3-h) bacterial attachment and inactivation, respectively. Extended-time electrochemical experiments (12 h) indicated that in all cases, the density of total deposited bacteria increased almost linearly with time and that the rate of bacterial adhesion was decreased 8- to 10-fold when an electric potential was applied. In summary, this study provides a fundamental rationale for the selection of CNM as cathode coatings and electric potential to reduce microbial fouling.

Biofilm formation is ubiquitous in aquatic environments and is undesirable for industrial systems, such as heat exchangers and ship hulls (1), as well as for engineered environmental systems, such as membrane filters (2) and water distribution pipelines. A critical initial stage of biofouling involves microorganism adhesion and formation of the primary slime layer that allows for continued biofilm development (3, 4). Thus, if initial microorganism adhesion is reduced, continued biofilm development may be slowed as well.

Continuous research efforts have been devoted to microbial fouling control, from the development of antimicrobial surfaces (5) to the disturbance of bacterial biofilm ecology by quorum sensing (6, 7). With regard to antimicrobial surfaces, the interfacial energy between a surface and water has been identified as a key factor in microbial adhesion, and hydrophilic surfaces generally hinder protein adsorption and, in turn, reduce biofouling (8). A highly charged cationic surface has also been demonstrated to kill bacteria and reduce fouling (9). However, since microbes have a complex and species-dependent surface chemistry, a permanently modified surface will not reduce biofouling for all microbes, and decreased antifouling performance is often observed in complex environments. One solution may be active biofouling reduction that can be tuned *in situ* to reduce biofouling for a range of species. Active chemical fouling reduction typically relies on the slow release of biocides from a surface (5), yet this method raises many environmental concerns and is restricted to a limited lifetime after the majority of the biocide is released. In contrast, photo- or electrochemical methods are among the most effective, easily automated, and environmentally friendly ways to reduce biofouling (10, 11), since the amount and time-dependent release of chemicals can be controlled via a feedback loop. Photo- and electrochemical biofouling reduction studies can be broadly divided into two categories: fundamental mechanism and novel material investigations.

With regard to the electrochemical mechanism of biofouling reduction, the influence of an electric current or potential on bacterial adhesion (12), detachment (10, 13–15), and inactivation (15–17) has been widely examined. The most commonly accepted theories are that the cathode repels bacteria via electrostatic interactions and the anode inactivates bacteria through direct and indirect oxidation (4, 18). However, some of the fundamental phenomena are still not clearly understood. For instance, Kerr et al. (12) observed reduced cathodic bacterial attachment; however, the magnitude of reduction was independent of the cathode potential, in disagreement with the classical electrostatic repulsion model, i.e., the Derjaguin–Landau–Verwey–Overbeek (DLVO) theory. Limited attention has been paid to the possibility of cathodic surface disinfection, e.g., the reduction of O_2 to reactive oxygen species (ROS). Also, most of the electrochemical biofouling reduction literature provides only qualitative relations between fouling reduction performance and electrochemical parameters. Therefore, one primary objective here is to provide (semi)quantitative relationships between bacterial attachment/

Received 19 February 2015 **Accepted** 30 April 2015

Accepted manuscript posted online 8 May 2015

Citation Zhang Q, Nghiem J, Silverberg GJ, Vecitis CD. 2015. Semiquantitative performance and mechanism evaluation of carbon nanomaterials as cathode coatings for microbial fouling reduction. Appl Environ Microbiol 81:4744–4755. doi:10.1128/AEM.00582-15.

Editor: S.-J. Liu

Address correspondence to Chad D. Vecitis, vecitis@seas.harvard.edu.

Supplemental material for this article may be found at http://dx.doi.org/10.1128/AEM.00582-15.

doi:10.1128/AEM.00582-15

inactivation on the cathode surface and electrochemical parameters.

Recent electrochemical biofouling research has also focused on the synthesis and application of novel electrode materials. Electrochemistry occurs at the electrode-electrolyte interface, and thus, for nonconductive surfaces, a conductive coating is required. Carbon-based materials, such as carbon black (CB) and graphite doped in a polymer matrix (17, 18), have been used previously as electrode-coating materials because they are stable and inexpensive. More recently, the investigation of engineered carbon nanomaterials (CNM), such as carbon nanotubes (CNT), has shown promise for electrochemical biofouling reduction due to superior antifouling properties, i.e., increased cytotoxicity and conductivity (19, 20). The nanosize also allows for dispersion in a range of matrices and a reduced material demand (21). For instance, de Lannoy et al. (2013) dispersed CNT into a thin polyamide film (~50 nm) to produce electrically conductive polymer-nanocomposite nanofiltration membranes that significantly reduced biofilm formation (22). Nevertheless, there is more to exploit in this area, since CNT properties can be tuned via chemical modification to increase cytotoxicity (23–25) and conductivity (26). It is also of interest to compare CNT with conventional CNM, such as CB, and emerging CNM, such as graphene or reduced graphene oxide (rGO), since CB, CNT, and rGO have varied dimensions on the nanoscale, and in turn, the coating morphologies are different. Thus, another primary objective of this research is to compare the levels of electrochemical biofouling reduction by engineered carbon nanomaterial coatings with different structures and surface chemistries.

Here *Pseudomonas fluorescens* is used as a representative bacterium for bacterial adhesion and potential biofilm development (27–29), and three materials—CNT, CB, and rGO—are utilized as the cathodic coatings on a Ti substrate for electrochemical biofouling reduction. All experiments were carried out in an artificial aqueous environment consisting of a 0.9% NaCl saline solution containing a 1/8 dilution of tryptic soy broth (TSB); this is a relatively nutritious aqueous condition compared to natural environments but is close to some extreme environments, such as food-processing wastewaters, where severe biofouling may take place. A comparison of potential aqueous conditions is given in Table S1 in the supplemental material. First, bacterial adhesion and inactivation on the CNM coatings in the absence of an applied potential were evaluated as a control for electrochemical fouling reduction. Next, a total voltage of −0.4 to −2.0 V was applied between the CNM-coated Ti cathode and the counterelectrode (carbon cloth anode), and the density of the bacteria deposited on the surface and the percentage of inactivation were semiquantitatively correlated with the electrode potential, current density, and hydrogen peroxide generation. Finally, extended electrochemical antibiofouling experiments were completed over 12 h to evaluate the dynamics of electrochemical microbial fouling reduction.

MATERIALS AND METHODS

Materials. Carbon nanotubes (C-grade; multiwall; powder and bulk paper) were purchased from NanoTechLabs, Inc. (Yadkinville, NC). Oxidized CNT (O-CNT) were prepared by sparging O_3 (5 to 10 mg liter^{-1}) into an NaOH solution (pH 10) and filtering the O_3-NaOH solution through CNT buckypaper in a commercial filtration casing (Whatman) while applying an anodic current of 3.2 mA cm^{-2} (40 mA total; effective filtration area, 12.5 cm^2; total voltage ranged from 4 to 8 V) for 60 min using a direct-current (DC) power supply (E3646A; Agilent). The O-CNT were annealed at 600°C (in a Thermolyne 21100 tube furnace) under an inert (Ar) atmosphere for 30 min to produce oxidized-annealed CNT (OA-CNT) (24). CB (Vulcan XC 72-R) was kindly donated by Cabot (Boston, MA) and was used as received. Reduced graphene oxide (rGO) was used as a representative 2-dimensional (2D) carbon nanomaterial; it was synthesized using a modified Hummers' method and was subsequently photoreduced by previously reported methods (30). A Nafion 117 solution (~5% in a mixture of lower aliphatic alcohols and water) and formaldehyde (35% in water) were purchased from Sigma-Aldrich (St. Louis, MO). *P. fluorescens* ATCC 700830 (ATCC, Manassas, VA) was utilized in the microbial attachment and inactivation experiments. Bacto tryptic soy broth (TSB; Becton Dickinson), NaCl (reagent grade), isopropyl alcohol (IPA), and ethanol (EtOH) (laboratory grade) were purchased from VWR International (West Chester, PA). The fluorescence staining reagents 4′,6-diamidino-2-phenyindole dilactate (DAPI) and propidium iodide (PI) were acquired from Life Technologies (Grand Island, NY). Deionized (DI) water (>18 MΩ) was produced by a Nanopure Infinity ultrapure water system (Barnstead/Thermolyne) and was used to prepare all solutions and to rinse containers.

Coating of the Ti electrode with carbon nanomaterials. The CNT, O-CNT, and OA-CNT were first dispersed in IPA with Nafion by probe ultrasonication and were then used to dip-coat a Ti substrate (31, 32). Briefly, 20 mg of CNT and 400 μl of the 5% Nafion solution were added to 20 ml of IPA and were ultrasonicated (Branson Sonifier S450-D) at 20 W (1,000 W liter^{-1}) for 15 min. The solution was covered with a piece of aluminum foil to avoid excessive solvent evaporation. Similar procedures were followed for CB and rGO dispersions, except that the concentration of the carbon material was increased from 1 to 5 mg ml^{-1} (with the same carbon/Nafion ratio) to ensure full surface coverage. The CNM dispersions were then allowed to cool to room temperature. The Ti coupons (length, width, and thickness, 4 by 2 by 0.15 cm, respectively) used as the electrode substrate were first polished with sandpaper (413Q; grit rating, 220; 3M), then placed in an ultrasonication bath (Branson 2100) for 5 min to remove attached particles, rinsed with copious amounts of tap water, DI water, and EtOH in series, and finally dried with compressed air. The clean Ti coupons were coated by immersion in freshly prepared CNM solutions for 5 s and were then hung vertically in an oven at 60°C for 2 min. The coated electrodes were kept in sterile containers until bacterial experiments or material characterization was completed.

Bacterial attachment experiments. *P. fluorescens* was cultured in TSB at 30°C and was harvested at the mid-exponential phase (18 h). After centrifugation and resuspension twice in a 0.9% NaCl saline solution, the bacterial stock solution was diluted to an optical density at 600 nm (OD_{600}) of 0.15 in saline solution (~10^8 ml^{-1} according to fluorescence microscopy enumeration). Finally, 1/8 the volume of TSB was added to the bacterial saline solution to provide essential nutrients, and the resulting solution contained 2.1 g liter^{-1} pancreatic casein digest, 0.4 g liter^{-1} papaic soybean digest, 0.3 g liter^{-1} dextrose, 0.3 g liter^{-1} K_2HPO_4, and 9.6 g liter^{-1} NaCl.

A scheme of the setup of the bacterial attachment experiment is displayed in Fig. 1, and a photograph of the system is shown in Fig. S1 in the supplemental material. Approximately 25 ml of the bacterial suspension was added to a 30-ml glass beaker and was maintained at 30°C using a water bath. The suspension was agitated by a magnetic stir bar at 90 rpm. The electrochemical experiments were carried out using the classical two-electrode system. The CNM-coated electrode was used as the working electrode, and a piece of carbon cloth (Carbon Cloth Plain [CCP]; product code CCP-30; length, width, and thickness, 4 by 2 by 0.02 cm, respectively; Fuel Cell Earth, Wakefield, MA) was used as the counter electrode. The two electrodes were prewetted with a 10:90 (vol/vol) EtOH–DI water solution to eliminate air bubbles, rinsed with DI water, and then fixed on a glass slide with rubber bands prior to insertion into the bacterial suspension. The distance between the electrodes was 1.2 cm, and the total applied voltage (−0.4 to −2.0 V) was controlled by a DC power supply (E3646A;

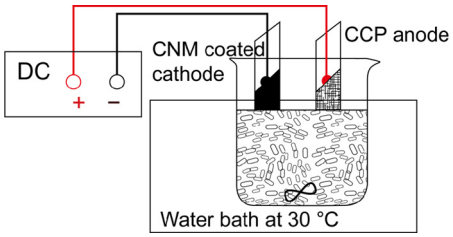

FIG 1 Schematic of the experimental setup for the examination of bacterial adhesion and inactivation. Typically, the Ti coupon with a CNM coating was used as the cathode, and the CCP was used as the anode. The bacterial solution was placed in a water bath (30°C) and was agitated with a magnetic bar at 90 rpm.

Agilent). The sign given to the total voltage (− or +) indicates the polarity of the CNM-coated electrode. In the majority of the experiments, the CNM had a negative polarity. The cathode potential (measured against the standard reference electrode [1 M Ag/AgCl]) was −0.3 to −1.2 V over the total voltage range of −0.4 to −2.0 V. The current of the system was monitored by a digital multimeter (34401A; Agilent). In general, the experiments to evaluate the effects of CNM coating materials and electrochemical parameters on *P. fluorescens* attachment and inactivation lasted 3 h. For the investigation of extended bacterial attachment and inactivation kinetics, the electrode surface was examined at 0.5, 3, 6, and 12 h. All bacterial attachment experiments were completed at least in duplicate, and two noncharged samples were analyzed for each batch of bacterial solution as a control.

After incubation of the electrodes in a bacterial solution in the absence or presence of an electric potential, the cathode was removed from the solution and was first rinsed to remove the nonattached bacteria by immersion in ~5 ml of saline solution with light agitation for 30 s. Subsequently, the cathode was quickly and lightly wiped with a paper pad to remove excess solution. Finally, the cathode was placed in a beaker containing 10 ml of saline solution and was vortexed at ~1,500 rpm (vortex mixer, model 58816-121; VWR) for 2 min. Disposable sterile or autoclaved containers were used to handle all solutions. Preliminary experiments (see Table S2 in the supplemental material) indicated that 2 min of vortexing was able to recover >95% of the bacteria from the coupon while retaining a percentage of inactivated bacteria similar to that found upon direct fluorescence observation. A fraction of the vortexed solution was then vacuum filtered onto a 0.2-μm gray polycarbonate membrane (Sterlitech, Kent, WA) and was stained with PI (to detect cells with compromised membranes; excitation/emission at 535/617 nm) for 10 min and with DAPI (to detect total cells; excitation/emission at 358/461 nm) for 5 min. The volume of the filtered solution was controlled such that there were 100 to 300 cells in the field of view (278 by 200 μm). The stained samples were quantified using an epifluorescence microscope (Olympus BX60) with a 40× objective lens. At least 5 images of random locations on each filter were recorded by a digital camera (Spot RT color camera; Diagnostic Instruments) for cell enumeration. The density of the bacteria on the original cathode was calculated using the equation below:

$$d_{\text{coating}} = N \times \left(\frac{A_{\text{filter}}}{A_{\text{photo}}}\right) \times \left(\frac{V_{\text{vortex}}}{V_{\text{filter}}}\right) \times \left(\frac{1}{A_{\text{vortex}}}\right)$$

where d_{coating} (expressed as the number of bacteria per square centimeter) is the density of the bacteria on the CNM electrode; N (dimensionless) stands for the bacterial counts from epifluorescent images; A_{filter}, A_{photo}, and A_{vortex} (expressed in square centimeters) are the areas of the polycarbonate membrane, the microscope image, and the coated sample for vortexing, respectively; and V_{vortex} and V_{filter} (expressed in milliliters) are the volume of bacterial solution vortexed and the volume filtered onto the polycarbonate membrane for cell counting, respectively.

Quantification of cathodic H_2O_2 electrogeneration. The potential contribution of electrochemical ROS to the loss of bacterial viability was examined by measuring cathodic H_2O_2 production. During cathodic electrolysis, H_2O_2 can be generated by reducing dissolved oxygen (33, 34), and H_2O_2 is known to be detrimental to bacteria (35, 36). To promote H_2O_2 generation and avoid loss via reaction with bacteria or broth, the electrodes were immersed in a 0.9% NaCl saline solution that was sparged with pure oxygen in the absence of bacteria and broth. Voltages similar to those used in the bacterial attachment/inactivation experiments were applied for 5 min. The solution was also more vigorously (120 rpm) stirred to ensure the dispersion of the reactive oxygen species so as to prevent further reduction to the hydroxyl radical or water. After 5 min of electrolysis, 1 ml of the solution was removed for H_2O_2 analysis by the ammonium molybdate-iodide method (37).

Characterization of CNM surface coatings. The CNM surface coatings were characterized by scanning electron microscopy (SEM), atomic force microscopy (AFM), and X-ray photoelectron spectroscopy (XPS). The contact angles and conductivities of CNM surface coatings were also measured.

SEM was carried out on a Zeiss UltraPlus field emission SEM (FESEM). Surface images were taken to compare the nanostructures of the different coatings, and cross-sectional images were utilized to determine the coating thickness. The surface morphology was also characterized by AFM (on an Asylum-1 MFP-3D AFM system) to determine surface roughness (estimated from a sample area of 1.5 by 1.5 μm). SEM was also used to examine bacterial morphology, especially the possible change to cell appendages on the CNT coating without or with total voltage after 3 and 12 h of contact. The samples were prepared by rinsing for 30 s in saline solution to remove the nonattached cells, placed in a sealed container with formaldehyde for vapor fixation (12 h), dehydrated in 40-to-100% EtOH–DI solutions, and finally completely dehydrated with a critical point dryer (931 GL 2.5; Tousimis).

XPS was carried out on a Thermo Scientific K-Alpha XPS. A survey scan was used to determine elemental ratios, and individual-element scans of C and O were used to determine individual functional group ratios. Casa XPS software was utilized to quantify the XPS data using Gaussian components after a Shirley background subtraction. The XPS peaks are deconvoluted into four categories; 284.4 to 285.3 eV for the sp^2- and sp^3-hybridized carbon atoms (C=C, C—C, or C—H) and 286.4 to 286.6 eV, 287.3 to 287.4 eV, and 288.8 to 289.3 eV for carbon atoms bound to oxygen atoms via one (C—O), two (C=O), and three (O—C=O) bonds, respectively (38–40). The contact angles of DI water with the clean CNM coating and with CNT coatings after bacterial experiments (dried) were measured using a goniometer (ramé-hart model 190 CA) via the sessile drop technique. At least 2 random samples were analyzed, and at least 12 measurements were performed on each sample.

For the conductivity measurement, a clean glass slide (VWR Superfrost Plus Micro Slide) was dip-coated with the CNM by following the procedure used for the polished Ti substrates. The sheet resistance of the coatings was determined with a conductivity analyzer (Keithley model 2635A System SourceMeter) using the four-point probe method. The bulk resistivity was calculated by multiplying the measured sheet resistance by the film thickness (as characterized by SEM cross-sectional images).

RESULTS

Material characterization. The physical-chemical properties of the CNM coating materials and the coatings are listed in Tables 1 and 2, respectively. SEM images of the CNT, O-CNT, CB, and rGO coatings are displayed in Fig. 2. Photographs of an uncoated polished Ti coupon and of Ti coupons with different CNM coatings are shown in Fig. S2 in the supplemental material.

The CNT surface chemistry is altered by the ozone-electrochemical oxidation and annealing treatments. The O/C ratio of the pure CNM increased from 0.00 for CNT to 0.09 for O-CNT, while that for the corresponding coating with Nafion increased from 0.18 to 0.25. The water contact angle of the O-CNT coating

TABLE 1 Physical-chemical properties of carbon nanomaterials

Carbon nanomaterial (without Nafion)	O/C ratio	Curve-fitting result of C(1s) spectra[a]				Main dimensions[b]
		C=C, C—C, or C—H	C—O	C=O	O=C—O	
CNT	0.004	1.000	N/D[c]	N/D	N/D	1D; D = 15 nm; L = 100 μm[d]
O-CNT	0.092	0.882	N/D	N/D	0.118[e]	D is similar to that of CNT; L is as short as 1 μm
OA-CNT	0.054	0.956	0.044	N/D	N/D	D and L are similar to those of O-CNT
CB	0.015	1.000	N/D	N/D	N/D	3D; spherical; D = 60 nm
rGO	0.404	0.531	N/D	0.399	0.070	2D; flake; L/W is 1 μm and thickness is 1.5 nm[f]

[a] Values are proportions of C with each type of bond. There are some discrepancies between the O/C analysis and the deconvolution of the C(1s) spectra, and the difference was within 30% for O-CNT, OA-CNT, and rGO. For reference to the two methods used, the XPS files for the rGO sample can be found in Fig. S3 in the supplemental material. Since the former data are directly from measurement and the latter are based on curve fitting, the former O/C ratio should be more reliable and have higher accuracy.
[b] D, diameter; L, length; W, width.
[c] N/D, none detected (<0.001) from the curve-fitting result of the C(1s) spectra.
[d] According to supplier specifications.
[e] A proportion of the carbon atoms (0.055) is fitted at the peak of 290.9 eV (C—F bond), likely from contamination on the sample surface by the fluorinated tubing in the oxidization system, and is not listed in this table.
[f] See reference 30.

(129.6 ± 3.0°) was slightly decreased from that of the CNT coating (135.8 ± 2.1°). Annealing the O-CNT at 600°C for 30 min under inert conditions to make OA-CNT reduced the O/C ratio without Nafion to 0.05 but slightly increased the O/C ratio of the coating with Nafion to 0.27 (likely due to improved interactions of OA-CNT with Nafion) and increased the contact angle of the coating to 134.5 ± 3.7°. The CNT functional groups are also different according to the deconvolution of the XPS C(1s) spectra. The pristine CNT contains minimal oxygen groups, and the O-CNT has 0.12 of carbon atoms highly oxidized in the form of O—C=O (higher than the O/C ratio of 0.09 due to the discrepancy between different analysis methods). After annealing, 0.044 of the carbon atoms on OA-CNT are bound to oxygen groups via one bond (C—O).

The morphology of the CNT coatings is influenced by oxidative and thermal treatments. As received, the CNT have a diameter of 15 to 20 nm and a length of 100 μm (41). The O-CNT are shorter than the CNT; some tube lengths around 1 μm can be observed by SEM (Fig. 2). The CNT coating has a nanoscale surface roughness of 2.86 nm, and the O-CNT coating has a nanoscale surface roughness of 4.58 nm based on the AFM estimation from an area of 1.5 by 1.5 μm (roughly the projection area of a single bacterium). The greater nanoscale roughness of the O-CNT is likely related to their shorter length, the increased number of tips, and the addition of functional groups. No dimensional changes to the individual tubes was observed for the OA-CNT relative to the O-CNT, yet the nanoscale surface roughness of the OA-CNT coating decreased to 3.41 nm, likely due to the removal of functional groups on the CNT tips or walls (42). The CNT, O-CNT, and OA-CNT coatings have similar thicknesses of 150 ± 5, 155 ± 5, and 120 ± 5 nm, respectively.

The other CNM, i.e., CB and rGO, are quite different from the CNT in both surface chemistry and coating morphology. CB is a hydrophobic material with an O/C ratio of 0.02. The contact angle of the CB coating was 124.5 ± 2.2°. rGO had the highest oxygen content (O/C ratio, 0.40, with 0.07 of the C in the form of O—C=O and 0.40 in the form of C=O), and the contact angle of the rGO coating, 96.9 ± 3.2°, was significantly lower than those of the other CNM coatings examined.

With regard to the morphology of the CB and rGO coatings, the nanoscale surface roughness of the CB coating is 4.82 nm, the

TABLE 2 Physical-chemical properties of the carbon nanomaterial coatings

Coating (with Nafion)	O/C ratio	Contact angle (°)	*Ra*[a] (nm)	Thickness (nm)	Electric resistivity (Ω cm)
CNT	0.180	135.8 ± 2.1	2.86	150 ± 5	0.029
O-CNT	0.254	129.6 ± 3.0	4.58	155 ± 5	0.042
OA-CNT	0.265	134.5 ± 3.7	3.41	120 ± 5	0.056
CB	0.119	124.5 ± 2.2	4.82	400 ± 5	0.950
rGO	0.270	96.9 ± 3.2	1.58	<5[b]	N/A[c]

[a] *Ra*, nanoscale surface roughness.
[b] Below the detection limit (~5 nm) by SEM observation of the cross section.
[c] NA, not applicable.

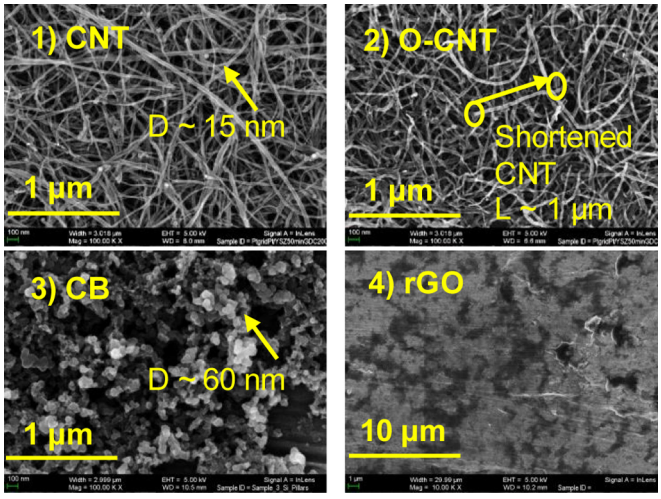

FIG 2 SEM images of the CNT, O-CNT, CB, and rGO coatings on the Ti substrate. D, diameter.

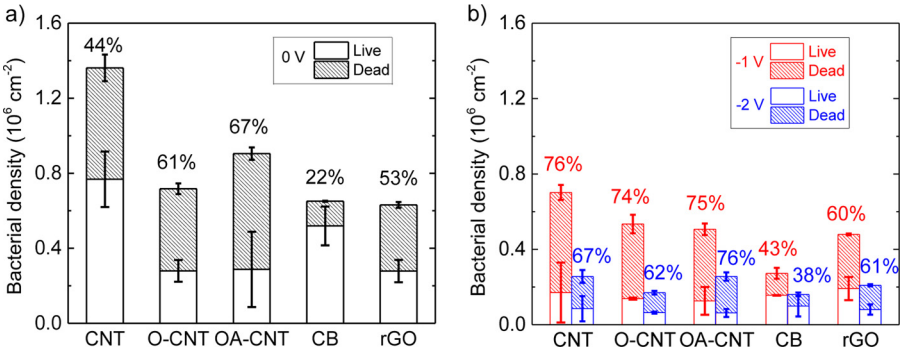

FIG 3 Densities of live/dead bacteria on CNM coatings in the absence (a) and presence (b) of a total voltage of −1.0 V or −2.0 V. The analysis was carried out after 3 h of incubation at 30°C in a 0.9% NaCl saline solution in 1/8 TSB. Shaded sections of bars represent the densities of inactivated bacteria, and open sections represent the densities of live bacteria. The percentage of inactivated bacteria is given above each bar.

highest among all the CNM utilized in this study, since CB consists of spherical nanoparticles with an average diameter of 60 nm. The CB coating is also much thicker (400 ± 5 nm) than the other CNM, which was necessary to achieve full surface coverage. rGO consists of flakes that are 1 μm wide and 1.5 nm thick and formed an extremely thin (<5 nm) and smooth (nanoscale surface roughness, 1.58 nm) coating on the Ti substrate.

The electrical resistivity of the CNT coating is the lowest, at 0.029 Ω cm. CNT oxidation and subsequent annealing increased the resistivity to 0.042 and 0.056 Ω cm, respectively. The CB coating has a bulk resistivity of 0.950 Ω cm, around 30-fold greater than that of pristine CNT. The resistivity of the rGO coating was nearly 10 orders of magnitude greater than that of the CNT coating due to the highly oxidized structure of rGO. However, the resistivity of the rGO coating cannot be measured accurately due to the lack of an accurate rGO thickness measurement, i.e., the coating was too thin to be accurately determined from the SEM cross-sectional image.

Bacterial attachment in the absence of an applied potential. The attachment and inactivation of *P. fluorescens* after 3 h of incubation in the absence of an applied potential were initially assessed as a control for the electrochemical experiments, and the results are presented in Fig. 3a.

P. fluorescens had the highest affinity for the CNT coating, for which the total density of attached bacteria was (1.36 ± 0.20) × 10^6 cm^{-2}; that density decreased to (0.90 ± 0.10) × 10^6 cm^{-2} and (0.72 ± 0.06) × 10^6 cm^{-2} for the OA-CNT and O-CNT coatings, respectively. The total densities of the bacteria on the CB and rGO coatings were (0.65 ± 0.03) × 10^6 cm^{-2} and (0.63 ± 0.07) × 10^6 cm^{-2}, respectively. The percentage of inactivation of the deposited bacteria is represented by the shaded section in the top portion of each bar in Fig. 3a, and the range from low to high was as follows: CB (22%), CNT (44%), rGO (53%), O-CNT (61%), OA-CNT (67%). Welch's *t* test of the total bacterial adhesion data showed that CNT had a significantly ($P < 0.05$) higher density of bacteria than the other coatings and that the density of bacteria on OA-CNT was higher than that on CB or rGO (see Table S3 in the supplemental material).

Statistical analysis was carried out by following a multilinear regression model to study the dependence of the density of adherent bacteria on the surface contact angle (as an indicator of surface hydrophobicity) and nanoscale roughness. The results are summarized in Table 3. The correlation coefficients for the contact angle (measured in degrees) and surface roughness (measured in nanometers) were 0.02 and −0.20, with *P* values of 0.08 and 0.12, respectively (i.e., there is a 0.08 chance for the null hypothesis that there is no dependence of the density of adherent bacteria on the contact angle to be true, whereas the chance for the null hypothesis for surface roughness to be true is 0.12). The intercept of the correlation was −1.13, and the corresponding *P* value was 0.24. Even though the *P* values for the two variables were greater than 0.05, the value generally used as the standard for a significant correlation, they were not far off. The overall R^2 value was 0.71, and thus, it is quite probable that there is a linear correlation between the total density of bacteria in the absence of an applied potential and the hydrophobicity and nanoscale roughness of the CNM coating.

Attachment of bacteria in the presence of an applied potential. After examination of the attachment of *P. fluorescens* to the control coatings in the absence of an electric potential, experiments on bacterial attachment as a function of total applied voltage were carried out using the CNM-coated Ti substrate as the cathode. The density and inactivation of bacteria at total voltages of −1.0 and −2.0 V after 3 h of incubation are shown in Fig. 3b. In general, the density of bacteria decreased (by 25 to 60% for −1.0 V and 67 to 90% for −2.0 V) and the percentage of inactivation increased (by 8 to 32% for −1.0 V and by 1 to 23% for −2.0 V) in the presence of an applied voltage relative to those for the noncharged controls. At −1.0 V, the range of average densities of *P. fluorescens* on the surfaces, from lowest to highest, was as follows: CB (0.27 × 10^6 cm^{-2}), rGO (0.48 × 10^6 cm^{-2}), OA-CNT (0.51 × 10^6 cm^{-2}), O-CNT (0.53 × 10^6 cm^{-2}), CNT (0.70 × 10^6 cm^{-2}); the corresponding percentages of bacteria inactivated were 43, 60,

TABLE 3 Multilinear regression results for the correlation of the density of bacteria on the CNM coating in the absence of an applied potential with the contact angle and nanoscale roughness

Parameter	Correlation		
	Coefficient	*P*	R^2
Variable 1, contact angle (°)	0.02	0.08	0.71
Variable 2, nanoscale roughness (nm)	−0.20	0.12	
Intercept, density of bacteria (10^6 cm^{-2})	−1.13	0.24	

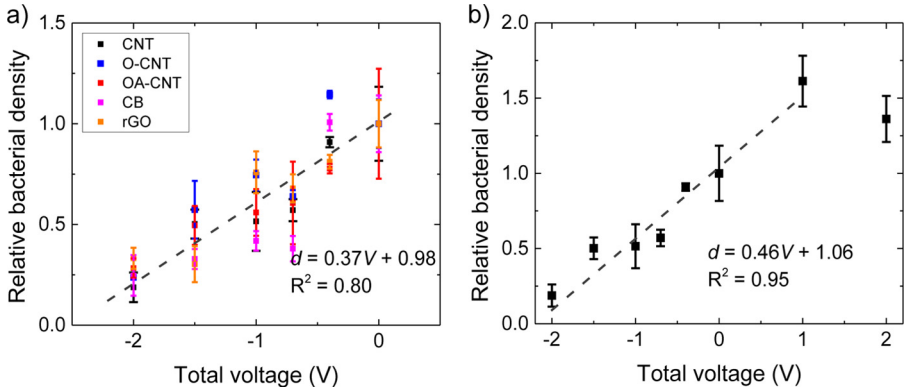

FIG 4 Total density of bacteria on surfaces normalized to the density of bacteria for noncharged controls. The analysis was conducted for all carbon nanomaterial coatings with a total applied voltage from −2.0 to 0 V (noncharged) (a), and for the CNT coating only with a total voltage of −2.0 to +2.0 V (b), after 3 h of incubation at 30°C in a 0.9% NaCl saline solution with 1/8 TSB.

75, 74, and 76%, respectively. At −2.0 V, the coatings had a further decreased number of total adherent bacteria ranging from 0.16×10^6 cm^{-2} for CB to 0.26×10^6 cm^{-2} for CNT and OA-CNT. The percentages of inactivation at −2.0 V were close to or less than those at −1.0 V and were as follows, from lowest to highest: CB (38%), rGO (61%), O-CNT (62%), CNT (67%), OA-CNT (76%).

The density of adherent bacteria on the various CNM coatings as a function of total voltage from −2.0 to 0 V after 3 h of incubation was normalized to that for noncharged controls as displayed in Fig. 4a. The *P* value of the one-way analysis of variance (ANOVA) of the normalized densities at different voltages for each CNM is <0.05 (even <0.01), indicating that the differences in the voltage-dependent normalized density of bacteria are significant. The combined data had a linear correlation ($d = 0.37V + 0.98$ and $R^2 = 0.80$, where d is the density of bacteria on the surface normalized to that on the control surface and V is the total applied voltage in volts) between the normalized density of bacteria and the applied voltage. To illustrate the effect of electric potential polarity on bacterial adhesion, positive total voltages of +1.0 and +2.0 V were also applied between the CNT coating and the CCP counter electrode (i.e., the CNT-coated electrode was used as the anode), and the relative density of bacteria is displayed in Fig. 4b. The linear correlation of the density of bacteria on the surface with the total applied voltage extended to positive surface charges up to +1.0 V, and upon the application of increased positive voltages, a decrease in total density of bacteria was observed (1.36 of the control at +2.0 V compared with 1.61 at +1.0 V).

The inactivation of *P. fluorescens* on the CNM coatings over a total voltage range of −2.0 to 0 V is displayed in Fig. 5 (black). To elucidate the underlying mechanism for the viability reduction of bacteria adhering to the cathode, the current density (blue) and H_2O_2 generation (red) are also displayed in Fig. 5. For purposes of comparison, the zero point of the direct current (blue) and that of H_2O_2 generation (red) were set at the same height as the percentage of inactivation for the control (uncharged) CNM coating, and the total range was kept consistent.

In contrast to the apparent linear decrease in total bacterial adhesion, the percentage of inactivation of bacteria had a nonlinear trend. For the CNT and CB coatings, the change in the percentage of inactivation with voltage was significant; the ANOVA *P* value was <0.05. The percentage decreased slightly from the control in the absence of potential to −0.4 V and increased back to the control level or higher at −0.7 V, but the deviation was <5%. For both materials, the greatest viability loss was observed at −1.0 V: 76% for CNT (compared with 44% for the control) and 43% for CB (compared with 22% for the control). At more-negative potentials, the percentage of inactivation first decreased at −1.5 V (to 54% for CNT and 33% for CB) and then increased at −2.0 V (to 67% for CNT and 38% for CB). For the O-CNT, OA-CNT, and rGO coatings, the percentages of inactivation of the controls were relatively high (61%, 67%, and 53%, respectively), and the variation with total voltage was relatively limited (the ANOVA *P* value was >0.05). In particular, for rGO, the percentage of inactivation for all the samples varied by only 13%. The greatest percentages of inactivation were observed at −1.5 V for O-CNT, OA-CNT, and rGO, at 78%, 81%, and 66%, respectively.

In general, the current density increased with increasing voltage. For the CNT, O-CNT, and OA-CNT coatings, the current density was as low as <0.01 mA cm^2 at total voltages of −0.4 to −1.0 V and increased to a maximum of ~0.15 mA cm^2 upon increases in the voltage from −1.0 to −2.0 V. The current increases for CB and rGO were less than those for the three CNT; the highest current densities, 0.10 and 0.07 mA cm^2, respectively, were observed at −2.0 V.

Despite the differing surface chemistries and morphologies of the CNM coatings, all displayed very similar trends toward H_2O_2 generation, which peaked at −1.5 V, corresponding to a cathode potential of around −0.9 V measured against the 1 M Ag/AgCl reference electrode (+0.23 V measured against a standard hydrogen electrode [see Fig. S4 in the supplemental material]). This is more negative than the theoretical dissolved O_2 reduction potential at a neutral pH of ~0.10 V measured against 1 M Ag/AgCl ($O_2 + 2H^+ + 2e^- \rightarrow H_2O_{2(aq)}$; $E^0 = 0.69$ V [Nernst equation]) (43) and previously reported values of −0.5 to −0.8 V measured against 1 M Ag/AgCl (44), likely to due to a higher overpotential from the Nafion coating hindering electron transfer. The maximum H_2O_2 concentration was ~0.01 mM after 5 min of electrolysis using saturated oxygen in the absence of bacteria and broth; thus, under the bacterial incubation conditions, the cumulative H_2O_2 generation will be less than 0.07 mM in 3 h. If one also considers possible cathodic H_2O_2 reduction pathways to the hydroxyl radical and water as well as H_2O_2 loss via reaction with the broth components, the final H_2O_2 concentration will be lower than the minimal concentrations observed to be toxic to bacteria

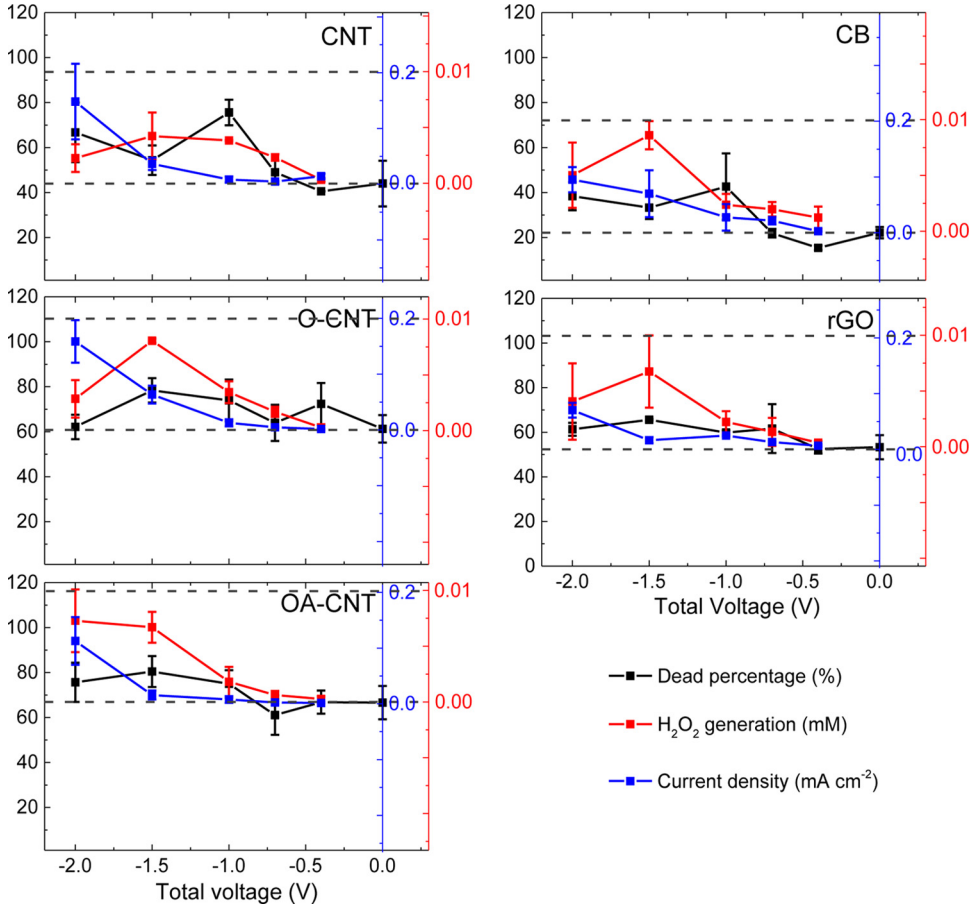

FIG 5 Loss of bacterial viability, direct-current density, and H_2O_2 generation for CNM coatings as functions of total applied voltage. The analysis was carried out with a total voltage of −2.0 to 0 V (noncharged) after 3 h of incubation at 30°C in a 0.9% NaCl saline solution with 1/8 TSB.

(≥0.15 mM) (45). In agreement with this expectation, <5% of the suspended bacteria were inactivated under an applied potential of −2.0 V.

A multilinear regression model was again applied in an attempt to examine quantitatively the dependence of bacterial inactivation (compared to that for uncharged controls) on the electric current and H_2O_2 generation. The results are summarized in Table 4. The overall correlation was not significant; R^2 is 0.12, and the P values of both variable inputs are >0.05. However, the correlation of the percentage of bacterial inactivation with H_2O_2 generation was notably greater than that with the current density, with 0.11 and 0.88 chances for the null hypothesis to be true, respectively.

The effect of electrochemistry on extended bacterial attachment and inactivation kinetics was also evaluated. The total densities of *P. fluorescens* cells on the CNT cathode coatings with total voltages of 0, −1.0, and −2.0 V after 0.5, 3, 6, and 12 h of incubation are displayed in Fig. 6a. In addition, *Escherichia coli* (ATCC 700830) was used in the up-to-12-h attachment experiments for comparison, as shown in Fig. S5 in the supplemental material. SEM analysis was carried out on the noncharged control and −1.0 and −2.0 V CNT coatings after 3 and 12 h of *P. fluorescens* incubation (Fig. 6b; see also Fig. S6 in the supplemental material).

Despite the inherent cytotoxicity of CNT, the density of bacteria on the control surface after 12 h in the absence of an electric potential, $(4.4 \pm 1.8) \times 10^6$ cm^{-2}, was significantly greater than that in the presence of an electric potential of −1.0 or −2.0 V, $(1.0 \pm 0.1) \times 10^6$ cm^{-2} or $(0.8 \pm 0.1) \times 10^6$ cm^{-2}, respectively. Thus, the application of an electric potential reduced the total density of bacteria to 0.18 of the control at −1.0 V and 0.14 of the control at −2.0 V after 12 h. For comparison, the relative total cell densities after 3 h of incubation were 0.45 and 0.16 of the control at −1.0 V and −2.0 V, respectively. In all cases, the total density of bacteria on the surface increased almost linearly with time. In the absence of an electric potential, the density of bacteria followed the equation $D_{0V} = 0.32t + 0.61$, where D is the density of bacteria in 10^6 cells per square centimeter (as distinguished from d, representing the density of bacteria normalized to that for the control), t is the incubation time in hours, and the slope indicates the rate of

TABLE 4 Multilinear regression results for the correlation between the increase in the percentage of dead bacteria over that for the controls with the current density and H_2O_2 generation

Parameter	Correlation		
	Coefficient	P	R^2
Variable 1, current density (mA cm^{-2})	−6.2	0.88	0.12
Variable 2, H_2O_2 concn (mM)	1,254.3	0.11	
Intercept, increase in % inactivation (%)	5.43	0.07	

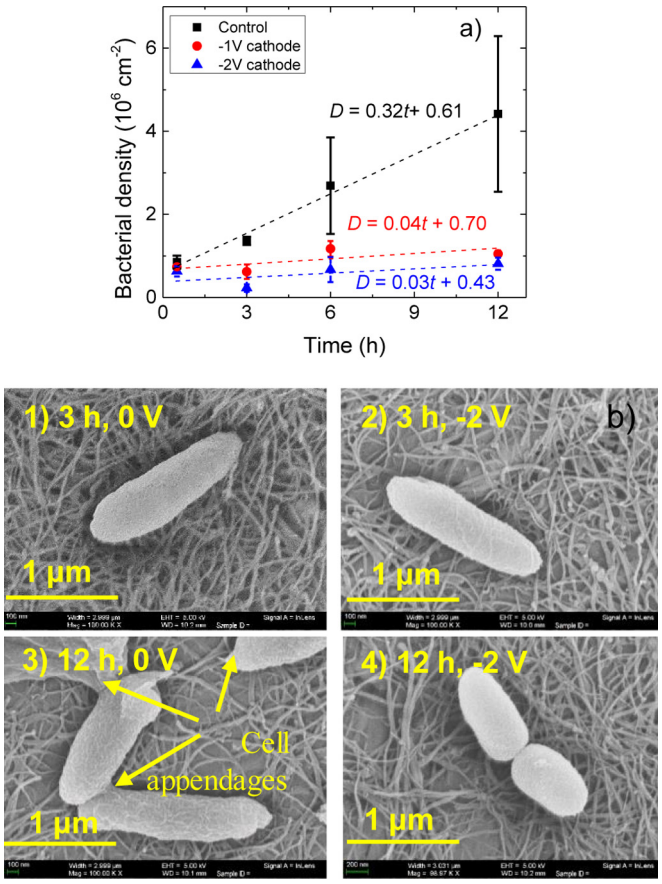

FIG 6 Bacterial growth on the CNT cathode as a function of total voltage and incubation time. (a) Total bacterial adhesion on the CNT surface with a total voltage of 0, −1, or −2.0 V after 0.5, 3, 6, or 12 h of incubation. (b) SEM images of bacterial morphology on the CNT cathode at 3 h and 0 V, 3 h and −2.0 V, 12 h and 0 V, and 12 h and −2.0 V, at 30°C in a 0.9% NaCl saline solution with 1/8 TSB.

increase in the density of adherent bacteria. The bacterial attachment kinetics was calculated as $D_{-1V} = 0.04t + 0.70$ in the presence of an electric potential at −1.0 V and as $D_{-2V} = 0.03t + 0.43$ at −2.0 V. Thus, the rate of bacterial adhesion on the CNT coating upon the application of −1.0 or −2.0 V was 8- to 10-fold less than that for the uncharged control, and in turn, the subsequent biofouling kinetics might also be reduced. According to the results shown in Fig. S5 in the supplemental material, *E. coli* generally had a much lower level of adhesion (5- to 10-fold) to the CNT surface (0.5×10^6 cells cm^{-2} after 12 h on the noncharged control) than *P. fluorescens*; however, the application of −1.0 or −2.0 V kept bacterial adhesion at a low level throughout the 12-h experiment ($<0.18 \times 10^6$ cm^{-2} or 0.16×10^6 cm^{-2}, respectively), confirming the electrochemical adhesion reduction trend observed in Fig. 6a.

Interestingly, the density of *P. fluorescens* cells on the cathode surface at both −1.0 and −2.0 V decreased from 0.5 h to 3 h of incubation, indicating that the initial adhesion of the bacteria is reversible (13). The underlying reason for the decrease is still not clear, but it may be due to the time necessary for the electric double layer to develop, i.e., the capacitive current stabilized after 15 min, delaying the attachment or detachment of organic matter or bacteria. Welch's *t* test showed that the application of −1.0 or −2.0 V to the electrode resulted in significantly lower total bacterial adhesion than that for the controls at 3 h and 12 h of incubation (see Table S4 in the supplemental material).

From the SEM analysis after 3 h of incubation (Fig. 6b), the intact bacterial cells look similar in the presence and absence of an electric potential, and no obvious cell appendages can be observed in either the 0-V (Fig. 6b1) or the −2.0-V (Fig. 6b2) experiment. However, after 12 h, the cells on the 0-V control surface (Fig. 6b3) have developed some appendage structure (46) adhering the cells to the surface as well as to each other, whereas the cells on the −2.0-V (Fig. 6b-4) cathode still have smooth surfaces.

DISCUSSION

Bacterial attachment in the absence of an electric potential. (i) Total density. The differences in bacterial attachment on the CNM coatings in the absence of an electric potential are functions of their hydrophobicity and surface roughness. Hydrophobic interactions have been demonstrated to drive cell adhesion to surfaces (47, 48), since bacteria have hydrophobic surface components, e.g., lipid bilayer membranes, despite commonly having an overall negative surface charge (49). Surface roughness on the micrometer or larger scale typically results in increased microbial adhesion due to an increased surface area (48) and enhanced bacterium-substrate interactions (50). However, recent studies have indicated that nanoscale surface roughness may reduce bacterial attachment (51, 52). The results of the multilinear regression model for the dependence of the density of attached bacteria on the contact angle and nanoscale roughness of the coating agree with the previous studies.

(ii) Percentage of inactivation. Upon contact with the CNM surface coating, a fraction of the bacteria will be inactivated due to membrane degradation and oxidative stress (53–55). It should also be noted that the surface of the polished Ti, and thus that of the CNM coating, is heterogeneous (for instance, the rGO-coated surface looked nonuniform under the SEM at the scale of micrometers [Fig. 2]), which may help account for the fact that only a fraction of the attached bacteria were inactivated.

For coatings with similar surface morphologies, i.e., the CNT, O-CNT, and OA-CNT coatings, the percentage of inactivation is a result of the material surface chemistry. Pasquini et al. (24) observed that oxidative acid treatment and subsequent annealing increased the cytotoxicity of the multiwall CNT due to increased CNT reactivity, which was closely related to the number of surface defect sites, such as oxygen-containing groups that change in speciation postannealing. Similarly, Akhavan and Ghaderi (56) examined the bacterial toxicity of graphene oxide and reduced graphene oxide and attributed the higher toxicity of the reduced graphene oxide to sharpened nanowall edges that had stronger interactions with the cell membrane and/or better charge transfer, resulting in increased cell membrane damage. Thus, the increase in the percentage of inactivation from CNT to O-CNT (44% to 61%) is due to the introduction of functional surface defects, e.g., surface oxy-groups, such as carboxylates or quinones, on the walls and tips of the tubes and, in turn, an increase in reactivity (24). Annealing can either remove the functional groups to reveal undecorated defects and sharper tips (42) or alter the speciation of the functional surface groups, resulting in higher or lower reactivity (57). Since the OA-CNT used here contain only C—O type functional groups according to XPS characterization, which are usually assigned to alcohols or ethers that have not been reported

to be highly reactive (39), it is likely that the former reason is responsible for the observed increase in the percentage of inactivation on OA-CNT (67%).

For materials with similar surface chemistries, Kang et al. (55) observed that CNT size (diameter) is a key factor governing antibacterial effects and that CNT with smaller diameters (single-wall) led to more irreversible cell morphology damage than CNT with larger diameters (multiwall). It has also been observed that the size of the graphene oxide aggregates is related to bacterial toxicity and that smaller aggregates had greater antibacterial activity (54). In this study, the CB and pristine CNT contain minimal surface oxygen functional groups. However, the CB particles are roughly spherical and have an average diameter of 60 nm, greater than the CNT diameter of 15 nm; thus, the CB has less potential for physical membrane perturbation, resulting in less bacterial inactivation (22%) than the CNT (44%). For comparison, Yang et al. (58) compared the toxicities of CB (diameter, 12 nm) and CNT (diameter, 8 nm) dispersions to primary mouse embryo fibroblasts and observed that CNT had a slightly higher cytotoxicity. Therefore, the diameter of CB versus that of CNT is likely the governing factor in cytotoxicity.

With regard to the rGO coating, increased bacterial toxicity might be expected due to the large amount of defect sites and the significantly smaller material dimension (thickness, 1.5 nm) of the graphene flakes compared to the other CNM evaluated here. However, the overlaid structure of the rGO coating (a smooth surface with a roughness of 1.58 nm) may not allow for sufficient contact between the rGO nano-edges and the bacterial cells, thus reducing antimicrobial activity. The percentage of inactivation by the rGO coating (53%) is greater than those for CB and CNT but less than those for O-CNT and OA-CNT.

Bacterial attachment in the presence of an applied potential. **(i) Normalized density.** The relative density of attached bacteria at 3 h decreased monotonically with an increasing applied negative working electrode potential. As mentioned briefly above, most bacteria are negatively charged at a neutral pH in an aqueous environment (49, 59); thus, the magnitude of the electrostatic interaction between the bacterial cell membrane and the cathode surface should decrease according to classical DLVO theory, which has been widely used to predict colloid and bacterial adhesion (59). A more-negative electrode potential will result in a more-negative surface charge and thus a stronger electrostatic repulsion between the electrode surface and bacterial cells. According to a DLVO energy calculation following a previously established method (60) (see Fig. S7 in the supplemental material), an energy barrier exists between the bacteria (−10.8 mV; measured with a ZEN 3600 Zetasizer [Malvern, United Kingdom]) and the cathode surface at all total voltages applied (−0.4 to −2.0 V).

Alternative mechanisms have also been proposed for bacterial desorption from an electrode surface. For instance, Poortinga et al. (2001) applied a potential of −0.9 V (−800 μA) to +1.9 V (800 μA) measured against a Ag/AgCl reference electrode to an indium tin oxide electrode of 21 cm^2 and found that the bacterial desorption probability increased with the observed current. Apart from the electrostatic interaction between the electrode surface and the bacteria, it was demonstrated that the charged surface also caused an electroosmotic effect, which resulted in bacterial movement in parallel with the electrode surface (14). In contrast, Kang et al. (2011) monitored the translational motion of bacteria on an anode surface using a particle-tracking method, but they found that the averaged mean square displacement of the bacterial cells was independent of the current density applied in the experimental range of 7.5 to 30 μA cm^{-2} (61). The current density in this study was intermediate between those for the two previous studies, ranging from −158 to +101 μA cm^{-2} for total voltages of −2.0 to +2.0 V; thus, an electroosmotic mechanism may also contribute to bacterial fouling reduction, especially for the observed decrease in *P. fluorescens* adhesion to the CNT coating at a total voltage of +2.0 V from that at +1.0 V (Fig. 5b). Yet the quantitative contribution of the electroosmotic force to bacterial adhesion is still not clear and requires further study.

(ii) Percentage of inactivation. Numerous studies have observed bacterial disinfection when an anodic current is applied (16, 17). For instance, when CNT were used as an anode, two possible bacterial inactivation pathways were identified: direct inactivation at the CNT surface and indirect inactivation by electrochemical production of Cl_2· or HOCl (62). However, cathodic bacterial inactivation, in particular for CNM, has not been well studied.

Indirect disinfection of the bacteria attached at the cathode via ROS formation is one possible mechanism (63). Hydrogen peroxide is a common cathodic electrolysis product from a CNM electrode via reduction of dissolved oxygen, and its presence is generally accepted as evidence for the production of more-reactive species, such as ·OH (63). According to the multilinear regression model of the dependence of bacterial inactivation on an electric current and H_2O_2 generation, the inactivation of *P. fluorescens* is significantly more likely related to H_2O_2 generation than to the total coulombs delivered to the electrode-solution interface, supporting a mechanism of indirect inactivation by ROS rather than direct inactivation by electron transfer from the cathode to the bacteria. However, it should be noted that the level of H_2O_2 generation during the 3-h experiments within the ambient environment is estimated to be lower than the toxic level if all the ROS are dispersed in the bulk solution, and in agreement, no significant percentage of inactivation (<5%) of the suspended bacteria was observed. One reason for this phenomenon is that the electrochemical reactions in a batch reactor are typically a mass transfer-limited process (64), and thus, H_2O_2 or other ROS are generated rapidly at the electrode-solution interface and will likely react before diffusing into the bulk solution, resulting in a relatively high interfacial ROS concentration.

The relatively weak correlation ($P = 0.11$) between the percentage of deposited bacteria that were inactivated and H_2O_2 generation may be related to alternative reaction mechanisms, for instance, the scavenging of ROS by broth ingredients. A notable decrease from the original contact angle of the CNT coating (135.8°) after 3 h of incubation in the bacterial solution with no electric potential (27.3°) or a total voltage of −2.0 V (30.2°) was observed here, suggesting that a layer of organic matter had accumulated on the CNT surface and might compete with the bacteria for reaction with cathodic ROS.

(iii) Adhesion kinetics. The enhanced microbial fouling inhibition, i.e., significantly (8- to 10-fold) reduced bacterial adhesion kinetics, on the CNM electrodes in the presence of an electric potential is related to the bacterial attachment process, which is generally described by two primary steps (47). The first step involves bacterial transport close to a surface, allowing for initial adhesion via van der Waals, electrostatic, and hydrophobic interactions. The next step is the irreversible attachment of the cells to

the surface by the production of extracellular polymeric substances (EPS). Thus, it is likely that the local cathode surface environment under −2.0 V not only causes a loss of bacterial viability but also inhibits the secretion of, or degrades, EPS and in turn reduces irreversible adhesion. Studies on this phenomenon are still limited, yet the recent research by Gall et al. (2013) on bacterial adhesion to an electrode surface using a quartz crystal microbalance with dissipation analysis may help elucidate the observations here. By monitoring the frequency shift from a reference resonance frequency as well as the dissipation of the piezoelectric crystal oscillation magnitude, information was collected on the rigidity/softness of the deposited bacteria. Subsequently, a model was proposed that on a negatively charged electrode surface, a positively charged electric double layer is developed, which causes bacterial cell surface appendages to aggregate, and in turn, the cell appears more rigid (65). Following this model, one can speculate that when exposed to a negative cathode potential, the bacterial EPS may not grow or expand as expected, and thus, bacterial adhesion is further reduced. The continued electrochemical fouling reduction over extended periods elucidates some of the discrepancies between the voltage dependence of bacterial adhesion and classical DLVO theory; for instance, the magnitude of reduction was independent of the cathode potential in long-term experiments lasting for a week (12).

It is also possible that the appendages observed on the control CNT surface after 12 h of incubation (Fig. 6b3; see also Fig. S61 and -2 in the supplemental material) were from cell wall extension (remains after cell division), which would indicate that some cells on the control (0-V) surface continue dividing and reproducing while those on the charged cathode surface are inhibited, resulting in slower growth kinetics on CNM electrodes in the presence of a negative potential. To test this hypothesis, a culturability test (see Table S5 in the supplemental material) was performed; it indicates that at total voltages of −1.0 and −2.0 V, the density of culturable bacteria was reduced by ~10-fold from that with the control CNT coating after 3 h of incubation.

Implications and applications of reductions in bacterial adhesion and viability by cathode potential. From the experimental results presented here, the use of CNM cathode coatings to electrochemically reduce bacterial attachment and viability seems quite promising. To guide the selection of CNM, the materials are compared below with regard to bacterial attachment on the noncharged control surface, electrochemical inhibition, and cost analysis.

First, bacterial attachment on the control coating in the absence of an applied potential is a key factor determining the fouling potential, which functions as the baseline for electrochemical biofouling reduction. The conventional material CB serves as a good coating material in this study due to its surface morphology. Pristine CNT has higher cytotoxicity for the deposited bacteria, but the relatively smooth and hydrophobic surface leads to greater bacterial adhesion. After oxidation and annealing, the CNT properties can be tailored to reduce bacterial adhesion and increase surface toxicity. The rGO coating has low bacterial adhesion as a result of the less hydrophobic surface and relatively high cytotoxicity. Improved design of the rGO surface orientation, for instance, to allow for more exposure of graphene edges to the bacteria (56), may increase the surface cytotoxicity. Thus, CNM surface properties should carefully considered in the design of an antibiofouling surface.

Second, electrochemical reduction of bacterial adhesion is much less dependent on the intrinsic properties of different CNM, and the application of a negative electric potential both reduces bacterial adhesion and increases bacterial inactivation. The electric conductivity of the coating material may be important when this technique is used to reduce the biofouling of a nonconductive material surface, since an even potential distribution across the lateral surface is required. Thus, the various CNT would yield a more effective coating, whereas the application of rGO may not be viable for electrochemical bacterial fouling reduction unless its conductivity can be greatly enhanced, e.g., via thermal/chemical reduction. It will also be of interest to develop new materials with high and/or selective electrochemical properties, e.g., a greater number of reactive oxy-defect sites, while still maintaining conductivity, allowing for increased inactivation of the attached bacteria.

Finally, the commercial and material costs should be taken into consideration in the selection of a surface coating material. On the one hand, CB still has a great advantage over the other materials in terms of commercial price and availability, i.e., the bulk industrial CB market price is less than US\$0.1 kg^{-1}. The industrial price for CNT has been brought down to as low as US\$100 kg^{-1} (66) according to a recent literature report, which will favor its growing application, while the commercial market for graphene production and application is still under development. On the other hand, the material cost for a uniform functional nano-thin coating greatly encourages the development of novel CNM coatings, especially graphene-like materials, since significantly less material is necessary to produce an electroactive coating (the rGO coating was <5 nm thick, while the CNT coatings were 100 to 150 nm thick, and the CB coating was 400 nm thick).

There are many possible applications for the use of a CNM coating as a cathode to reduce biofouling. For instance, a significant proportion of water pipes today are made of polyvinyl chloride (PVC), which is not conductive, and a CNM coating may serve as a conductive surface to electrochemically reduce fouling, especially for rich solutions, such as food and beverage wastewater. Another example is membrane filtration, where frequent backwashing (approximately every 30 min) is necessary to maintain membrane permeability in wastewater treatment facilities. If the kinetics of bacterial adhesion could be reduced 8- to 10-fold, one would expect reduced backwashing frequency and thus decreased operation and maintenance (O&M) costs.

Conclusion. *P. fluorescens* adhesion and inactivation on a Ti cathode coated with CNT, O-CNT, OA-CNT, CB, or rGO were systematically and semiquantitatively analyzed. For the CNM coatings in the absence of an applied potential, total bacterial adhesion is correlated with the hydrophobicity and nanoscale roughness of the surface coating, while the loss of bacterial viability is related to the CNM nanoscale dimensions and surface chemistry. For electrochemical biofouling reduction, the density of bacteria on the surface decreased linearly with increasing applied negative potential for all CNM-coated cathodes, indicating that electrostatic repulsion was the dominant mechanism. The electrochemical inactivation of the deposited bacteria was best correlated with H_2O_2 generation, and the inactivation was effective only against adherent rather than suspended bacteria, likely due to a high near-surface concentration of cathodic ROS. Extended-time (12-h) experiments indicated that the application of a negative potential to the CNT-coated electrode reduced the bacterial adhe-

sion kinetics by 8- to 10-fold, as well as the production of EPS or cell appendages by adherent cells, likely reducing irreversible attachment. In conclusion, the use of CNM as cathode-coating materials is a promising method for actively reducing microbial fouling, and the present study provides semiquantitative insight into the material properties and electrochemical parameters most relevant to biofouling reduction, which will provide fundamental support for future research and applications.

ACKNOWLEDGMENTS

We thank Ralph Mitchell for providing lab facilities for microbial experiments. We thank the Harvard University Center for Nanoscale Systems for SEM, AFM, and XPS. We thank Archana Vasanthakumar, Alice DeAraujo, and Kuichang Zuo for assistance with microbial analyses. We thank You Zhou for assistance with four-point conductivity measurements.

Q.Z. thanks Life Technologies for financial support.

REFERENCES

1. **Mattilasandholm T, Wirtanen G.** 1992. Biofilm formation in the industry—a review. Food Rev Int **8:**573–603. http://dx.doi.org/10.1080/87559129209540953.
2. **Baker JS, Dudley LY.** 1998. Biofouling in membrane systems—a review. Desalination **118:**81–89. http://dx.doi.org/10.1016/S0011-9164(98)00091-5.
3. **O'Neill TB, Wilcox GL.** 1971. The formation of a "primary film" on materials submerged in the sea at Port Hueneme, California. Pac Sci **25:**1–12.
4. **Hori K, Matsumoto S.** 2010. Bacterial adhesion: from mechanism to control. Biochem Eng J **48:**424–434. http://dx.doi.org/10.1016/j.bej.2009.11.014.
5. **Yebra DM, Kiil S, Dam-Johansen K.** 2004. Antifouling technology—past, present and future steps towards efficient and environmentally friendly antifouling coatings. Prog Org Coat **50:**75–104. http://dx.doi.org/10.1016/j.porgcoat.2003.06.001.
6. **Hentzer M, Riedel K, Rasmussen TB, Heydorn A, Andersen JB, Parsek MR, Rice SA, Eberl L, Molin S, Hoiby N, Kjelleberg S, Givskov M.** 2002. Inhibition of quorum sensing in *Pseudomonas aeruginosa* biofilm bacteria by a halogenated furanone compound. Microbiology **148:**87–102.
7. **Jayaraman A, Wood TK.** 2008. Bacterial quorum sensing: signals, circuits, and implications for biofilms and disease. Annu Rev Biomed Eng **10:**145–167. http://dx.doi.org/10.1146/annurev.bioeng.10.061807.160536.
8. **Krishnan S, Weinman CJ, Ober CK.** 2008. Advances in polymers for anti-biofouling surfaces. J Mater Chem **18:**3405–3413. http://dx.doi.org/10.1039/b801491d.
9. **Murata H, Koepsel RR, Matyjaszewski K, Russell AJ.** 2007. Permanent, non-leaching antibacterial surfaces—2: how high density cationic surfaces kill bacterial cells. Biomaterials **28:**4870–4879. http://dx.doi.org/10.1016/j.biomaterials.2007.06.012.
10. **van der Borden AJ, van der Werf H, van der Mei HC, Busscher HJ.** 2004. Electric current-induced detachment of *Staphylococcus epidermidis* biofilms from surgical stainless steel. Appl Environ Microbiol **70:**6871–6874. http://dx.doi.org/10.1128/AEM.70.11.6871-6874.2004.
11. **Shim S, Hong SH, Tak Y, Yoon J.** 2011. Prevention of *Pseudomonas aeruginosa* adhesion by electric currents. Biofouling **27:**217–224. http://dx.doi.org/10.1080/08927014.2011.554831.
12. **Kerr A, Hodgkiess T, Cowling MJ, Beveridge CM, Smith MJ, Parr ACS.** 1998. A novel technique to prevent bacterial fouling, using imposed surface potential. J Appl Microbiol **85:**1067–1072. http://dx.doi.org/10.1111/j.1365-2672.1998.tb05272.x.
13. **Poortinga AT, Bos R, Busscher HJ.** 2001. Reversibility of bacterial adhesion at an electrode surface. Langmuir **17:**2851–2856. http://dx.doi.org/10.1021/la001673y.
14. **Poortinga AT, Smit J, van der Mei HC, Busscher HJ.** 2001. Electric field induced desorption of bacteria from a conditioning film covered substratum. Biotechnol Bioeng **76:**395–399. http://dx.doi.org/10.1002/bit.10129.
15. **Hong SH, Jeong J, Shim S, Kang H, Kwon S, Ahn KH, Yoon J.** 2008. Effect of electric currents on bacterial detachment and inactivation. Biotechnol Bioeng **100:**379–386. http://dx.doi.org/10.1002/bit.21760.
16. **Nakasono S, Nakamura N, Sode K, Matsunaga T.** 1992. Electrochemical disinfection of marine bacteria attached on a plastic electrode. Bioelectrochem Bioenerg **27:**191–198. http://dx.doi.org/10.1016/0302-4598(92)87042-S.
17. **Nakasono S, Burgess JG, Takahashi K, Koike M, Murayama C, Nakamura S, Matsunaga T.** 1993. Electrochemical prevention of marine biofouling with a carbon-chloroprene sheet. Appl Environ Microbiol **59:**3757–3762.
18. **Matsunaga T, Nakayama T, Wake H, Takahashi M, Okochi M, Nakamura N.** 1998. Prevention of marine biofouling using a conductive paint electrode. Biotechnol Bioeng **59:**374–378. http://dx.doi.org/10.1002/(SICI)1097-0290(19980805)59:3<374::AID-BIT14>3.0.CO;2-E.
19. **Lam CW, James JT, McCluskey R, Arepalli S, Hunter RL.** 2006. A review of carbon nanotube toxicity and assessment of potential occupational and environmental health risks. Crit Rev Toxicol **36:**189–217. http://dx.doi.org/10.1080/10408440600570233.
20. **Kang S, Mauter MS, Elimelech M.** 2009. Microbial cytotoxicity of carbon-based nanomaterials: implications for river water and wastewater effluent. Environ Sci Technol **43:**2648–2653. http://dx.doi.org/10.1021/es8031506.
21. **Upadhyayula VK, Gadhamshetty V.** 2010. Appreciating the role of carbon nanotube composites in preventing biofouling and promoting biofilms on material surfaces in environmental engineering: a review. Biotechnol Adv **28:**802–816. http://dx.doi.org/10.1016/j.biotechadv.2010.06.006.
22. **de Lannoy C-F, Jassby D, Gloe K, Gordon AD, Wiesner MR.** 2013. Aquatic biofouling prevention by electrically charged nanocomposite polymer thin film membranes. Environ Sci Technol **47:**2760–2768. http://dx.doi.org/10.1021/es3045168.
23. **Pasquini LM, Hashmi SM, Sommer TJ, Elimelech M, Zimmerman JB.** 2012. Impact of surface functionalization on bacterial cytotoxicity of single-walled carbon nanotubes. Environ Sci Technol **46:**6297–6305. http://dx.doi.org/10.1021/es300514s.
24. **Pasquini LM, Sekol RC, Taylor AD, Pfefferle LD, Zimmerman JB.** 2013. Realizing comparable oxidative and cytotoxic potential of single- and multiwalled carbon nanotubes through annealing. Environ Sci Technol **47:**8775–8783. http://dx.doi.org/10.1021/es401786s.
25. **Gilbertson LM, Goodwin DG, Taylor AD, Pfefferle L, Zimmerman JB.** 2014. Toward tailored functional design of multi-walled carbon nanotubes (MWNTs): electrochemical and antimicrobial activity enhancement via oxidation and selective reduction. Environ Sci Technol **48:**5938–5945. http://dx.doi.org/10.1021/es500468y.
26. **Kim YJ, Shin TS, Choi HD, Kwon JH, Chung YC, Yoon HG.** 2005. Electrical conductivity of chemically modified multiwalled carbon nanotube/epoxy composites. Carbon **43:**23–30. http://dx.doi.org/10.1016/j.carbon.2004.08.015.
27. **Stoodley P, Lewandowski Z.** 1994. Liquid flow in biofilm systems. Appl Environ Microbiol **60:**2711–2716.
28. **Stoodley P, Wilson S, Hall-Stoodley L, Boyle JD, Lappin-Scott HM, Costerton J.** 2001. Growth and detachment of cell clusters from mature mixed-species biofilms. Appl Environ Microbiol **67:**5608–5613. http://dx.doi.org/10.1128/AEM.67.12.5608-5613.2001.
29. **Jackson G, Beyenal H, Rees WM, Lewandowski Z.** 2001. Growing reproducible biofilms with respect to structure and viable cell counts. J Microbiol Methods **47:**1–10. http://dx.doi.org/10.1016/S0167-7012(01)00280-9.
30. **Silverberg GJ, Pearce P, Vecitis CD.** 2015. Controlling self-assembly of reduced graphene oxide at the air-water interface: quantitative evidence for long-range attractive and many-body interactions. ACS Appl Mater Interfaces **7:**3807–3815. http://dx.doi.org/10.1021/am5087984.
31. **Wang J, Musameh M, Lin Y.** 2003. Solubilization of carbon nanotubes by Nafion toward the preparation of amperometric biosensors. J Am Chem Soc **125:**2408–2409. http://dx.doi.org/10.1021/ja028951v.
32. **Li J, Guo S, Zhai Y, Wang E.** 2009. High-sensitivity determination of lead and cadmium based on the Nafion-graphene composite film. Anal Chim Acta **649:**196–201. http://dx.doi.org/10.1016/j.aca.2009.07.030.
33. **Brillas E, Sirés I, Oturan MA.** 2009. Electro-Fenton process and related electrochemical technologies based on Fenton's reaction chemistry. Chem Rev **109:**6570–6631. http://dx.doi.org/10.1021/cr900136g.
34. **Campos-Martin JM, Blanco-Brieva G, Fierro JLG.** 2006. Hydrogen peroxide synthesis: an outlook beyond the anthraquinone process. Angew Chem Int Ed Engl **45:**6962–6984. http://dx.doi.org/10.1002/anie.200503779.
35. **Drogui P, Elmaleh S, Rumeau M, Bernard C, Rambaud A.** 2001.

Hydrogen peroxide production by water electrolysis: application to disinfection. J Appl Electrochem **31:**877–882. http://dx.doi.org/10.1023/A:1017588221369.
36. **Drogui P, Elmaleh S, Rumeau M, Bernard C, Rambaud A.** 2001. Oxidising and disinfecting by hydrogen peroxide produced in a two-electrode cell. Water Res **35:**3235–3241. http://dx.doi.org/10.1016/S0043-1354(01)00021-5.
37. **Kormann C, Bahnemann DW, Hoffmann MR.** 1988. Photocatalytic production of hydrogen peroxides and organic peroxides in aqueous suspensions of titanium dioxide, zinc oxide, and desert sand. Environ Sci Technol **22:**798–806. http://dx.doi.org/10.1021/es00172a009.
38. **Akhavan O.** 2010. The effect of heat treatment on formation of graphene thin films from graphene oxide nanosheets. Carbon **48:**509–519. http://dx.doi.org/10.1016/j.carbon.2009.09.069.
39. **Ago H, Kugler T, Cacialli F, Salaneck WR, Shaffer MSP, Windle AH, Friend RH.** 1999. Work functions and surface functional groups of multiwall carbon nanotubes. J Phys Chem B **103:**8116–8121. http://dx.doi.org/10.1021/jp991659y.
40. **Charlier JC, Arnaud L, Avilov IV, Delgado M, Demoisson F, Espinosa EH, Ewels CP, Felten A, Guillot J, Ionescu R, Leghrib R, Llobet E, Mansour A, Migeon HN, Pireaux JJ, Reniers F, Suarez-Martinez I, Watson GE, Zanolli Z.** 2009. Carbon nanotubes randomly decorated with gold clusters: from nano^{2}hybrid atomic structures to gas sensing prototypes. Nanotechnology **20**(37)**:**375501. http://dx.doi.org/10.1088/0957-4484/20/37/375501.
41. **Gao GD, Vecitis CD.** 2012. Reactive depth and performance of an electrochemical carbon nanotube network as a function of mass transport. ACS Appl Mater Interfaces **4:**6096–6103. http://dx.doi.org/10.1021/am301724n.
42. **Holloway AF, Wildgoose GG, Compton RG, Shao L, Green MLH.** 2008. The influence of edge-plane defects and oxygen-containing surface groups on the voltammetry of acid-treated, annealed and "super-annealed" multiwalled carbon nanotubes. J Solid State Electrochem **12:**1337–1348. http://dx.doi.org/10.1007/s10008-008-0542-2.
43. **Khataee A, Safarpour M, Zarei M, Aber S.** 2011. Electrochemical generation of H_2O_2 using immobilized carbon nanotubes on graphite electrode fed with air: investigation of operational parameters. J Electroanal Chem **659:**63–68. http://dx.doi.org/10.1016/j.jelechem.2011.05.002.
44. **Gao G, Zhang Q, Hao Z, Vecitis CD.** 2015. Carbon nanotube membrane stack for flow-through sequential regenerative electro-Fenton. Environ Sci Technol **49:**2375–2383. http://dx.doi.org/10.1021/es505679e.
45. **Imlay JA, Linn S.** 1986. Bimodal pattern of killing of DNA-repair-defective or anoxically grown *Escherichia coli* by hydrogen peroxide. J Bacteriol **166:**519–527.
46. **Ishii S, Koki J, Unno H, Hori K.** 2004. Two morphological types of cell appendages on a strongly adhesive bacterium, *Acinetobacter* sp. strain Tol 5. Appl Environ Microbiol **70:**5026–5029. http://dx.doi.org/10.1128/AEM.70.8.5026-5029.2004.
47. **Palmer J, Flint S, Brooks J.** 2007. Bacterial cell attachment, the beginning of a biofilm. J Ind Microbiol Biotechnol **34:**577–588. http://dx.doi.org/10.1007/s10295-007-0234-4.
48. **Donlan RM.** 2002. Biofilms: microbial life on surfaces. Emerg Infect Dis **8:**881–890. http://dx.doi.org/10.3201/eid0809.020063.
49. **Rosenberg M, Kjelleberg S.** 1986. Hydrophobic interactions: role in bacterial adhesion. Adv Microb Ecol **9:**353–393. http://dx.doi.org/10.1007/978-1-4757-0611-6_8.
50. **Taylor RL, Verran J, Lees GC, Ward AP.** 1998. The influence of substratum topography on bacterial adhesion to polymethyl methacrylate. J Mater Sci Mater Med **9:**17–22. http://dx.doi.org/10.1023/A:1008874326324.
51. **Puckett SD, Taylor E, Raimondo T, Webster TJ.** 2010. The relationship between the nanostructure of titanium surfaces and bacterial attachment. Biomaterials **31:**706–713. http://dx.doi.org/10.1016/j.biomaterials.2009.09.081.
52. **Mitik-Dineva N, Wang J, Truong VK, Stoddart P, Malherbe F, Crawford RJ, Ivanova EP.** 2009. *Escherichia coli*, *Pseudomonas aeruginosa*, and *Staphylococcus aureus* attachment patterns on glass surfaces with nanoscale roughness. Curr Microbiol **58:**268–273. http://dx.doi.org/10.1007/s00284-008-9320-8.
53. **Vecitis CD, Zodrow KR, Kang S, Elimelech M.** 2010. Electronic-structure-dependent bacterial cytotoxicity of single-walled carbon nanotubes. ACS Nano **4:**5471–5479. http://dx.doi.org/10.1021/nn101558x.
54. **Liu S, Zeng TH, Hofmann M, Burcombe E, Wei J, Jiang R, Kong J, Chen Y.** 2011. Antibacterial activity of graphite, graphite oxide, graphene oxide, and reduced graphene oxide: membrane and oxidative stress. ACS Nano **5:**6971–6980. http://dx.doi.org/10.1021/nn202451x.
55. **Kang S, Herzberg M, Rodrigues DF, Elimelech M.** 2008. Antibacterial effects of carbon nanotubes: size does matter. Langmuir **24:**6409–6413. http://dx.doi.org/10.1021/la800951v.
56. **Akhavan O, Ghaderi E.** 2010. Toxicity of graphene and graphene oxide nanowalls against bacteria. ACS Nano **4:**5731–5736. http://dx.doi.org/10.1021/nn101390x.
57. **Jürmann G, Tammeveski K.** 2006. Electroreduction of oxygen on multiwalled carbon nanotubes modified highly oriented pyrolytic graphite electrodes in alkaline solution. J Electroanal Chem **597:**119–126. http://dx.doi.org/10.1016/j.jelechem.2006.09.002.
58. **Yang H, Liu C, Yang DF, Zhang HS, Xi ZG.** 2009. Comparative study of cytotoxicity, oxidative stress and genotoxicity induced by four typical nanomaterials: the role of particle size, shape and composition. J Appl Toxicol **29:**69–78. http://dx.doi.org/10.1002/jat.1385.
59. **Hermansson M.** 1999. The DLVO theory in microbial adhesion. Colloids Surf B **14:**105–119. http://dx.doi.org/10.1016/S0927-7765(99)00029-6.
60. **Zhang Q, Vecitis CD.** 2014. Conductive CNT-PVDF membrane for capacitive organic fouling reduction. J Membr Sci **459:**143–156. http://dx.doi.org/10.1016/j.memsci.2014.02.017.
61. **Kang H, Shim S, Lee SJ, Yoon J, Ahn KH.** 2011. Bacterial translational motion on the electrode surface under anodic electric field. Environ Sci Technol **45:**5769–5774. http://dx.doi.org/10.1021/es200752h.
62. **Vecitis CD, Schnoor MH, Rahaman MS, Schiffman JD, Elimelech M.** 2011. Electrochemical multiwalled carbon nanotube filter for viral and bacterial removal and inactivation. Environ Sci Technol **45:**3672–3679. http://dx.doi.org/10.1021/es2000062.
63. **Jeong J, Kim JY, Yoon J.** 2006. The role of reactive oxygen species in the electrochemical inactivation of microorganisms. Environ Sci Technol **40:**6117–6122. http://dx.doi.org/10.1021/es0604313.
64. **Liu H, Vecitis CD.** 2012. Reactive transport mechanism for organic oxidation during electrochemical filtration: mass-transfer, physical adsorption, and electron-transfer. J Phys Chem C **116:**374–383. http://dx.doi.org/10.1021/jp209390b.
65. **Gall I, Herzberg M, Oren Y.** 2013. The effect of electric fields on bacterial attachment to conductive surfaces. Soft Matter **9:**2443–2452. http://dx.doi.org/10.1039/c2sm27270a.
66. **De Volder MF, Tawfick SH, Baughman RH, Hart AJ.** 2013. Carbon nanotubes: present and future commercial applications. Science **339:**535–539. http://dx.doi.org/10.1126/science.1222453.